MICROCOPY RESOLUTION TEST CHART

NATIONAL BUREAU OF STANDARDS-1963-A

USE OF DEPLETION-EDGE TRANSLATION FOR
HIGH SPEED MODULATION AND SWITCHING OF
LIGHTWAVES: YEAR-1

by
L.A. Coldren, A. Alping, X.S. Wu, T.R. Hausken,
T.C. Huang and J.R. Karin

DTIC
ELECTE
FEB 25 1987
S
D
D

DEPARTMENT OF ELECTRICAL AND COMPUTER ENGINEERING

UNIVERSITY OF CALIFORNIA   SANTA BARBARA, CALIFORNIA 93106

AD-A176 839

DTIC FILE COPY

USE OF DEPLETION-EDGE TRANSLATION FOR HIGH SPEED MODULATION AND SWITCHING OF LIGHTWAVES: YEAR-1

by

L.A. Coldren, A. Alping, X.S. Wu, T.R. Hausken,
T.C. Huang and J.R. Karin

AFOSR·TR· 87-0151

DTIC
ELECTE
FEB 2 5 1987
D

ADA176839

REPORT DOCUMENTATION PAGE

1a. REPORT SECURITY CLASSIFICATION	1b. RESTRICTIVE MARKINGS
Unclassified	

2a. SECURITY CLASSIFICATION AUTHORITY	3. DISTRIBUTION/AVAILABILITY OF REPORT
	Approved for public release;
2b. DECLASSIFICATION/DOWNGRADING SCHEDULE	distribution unlimited.

4. PERFORMING ORGANIZATION REPORT NUMBER(S)	5. MONITORING ORGANIZATION REPORT NUMBER(S)
	AFOSR-TR· 8 7 - 0 1 5 1

6a. NAME OF PERFORMING ORGANIZATION	6b. OFFICE SYMBOL (If applicable)	7a. NAME OF MONITORING ORGANIZATION
Univ. of CA (Santa Barbara)		AFOSR

6c. ADDRESS (City, State and ZIP Code)	7b. ADDRESS (City, State and ZIP Code)
Dept. of Electrical Engineering	Bolling AFB DC 20332
Santa Barbara, CA 93106	

8a. NAME OF FUNDING/SPONSORING ORGANIZATION	8b. OFFICE SYMBOL (If applicable)	9. PROCUREMENT INSTRUMENT IDENTIFICATION NUMBER
same as 7a	NE	same as 5

8c. ADDRESS (City, State and ZIP Code)	10. SOURCE OF FUNDING NOS.			
	PROGRAM ELEMENT NO.	PROJECT NO.	TASK NO.	WORK UNIT NO.
same as 7b	61102f	2305	B1	

11. TITLE (Include Security Classification)
Use of depletion edge translation for high-speed
modulation and switching of lightwaves"

12. PERSONAL AUTHOR(S)
Drs. Larry Coldren

13a. TYPE OF REPORT	13b. TIME COVERED	14. DATE OF REPORT (Yr., Mo., Day)	15. PAGE COUNT
ANNUAL REPORT	FROM 1 Aug 85 TO 7-31-86	OCT. 86	24

16. SUPPLEMENTARY NOTATION

17.	COSATI CODES		18. SUBJECT TERMS (Continue on reverse if necessary and identify by block number)
FIELD	GROUP	SUB. GR.	

19. ABSTRACT (Continue on reverse if necessary and identify by block number)

This report describes initial results from the investigation of a new device concept for optical modulators and switches. Applications may be found in optical communication, IC-interconnection and optical computing. The basic concept involves combining and maximizing several effects that can occur in the depletion region of a semiconductor pn-junction to change the index of refraction therein. As a reverse-bias is applied to a properly designed device, the depletion region gets wider and in the index shift within it gets larger relative to the surrounding material. The result is that more efficient, compact and potentially higher-speed devices can be realized, since most optical modulation and switching concepts rely upon a change in the index of refraction in some region. Initial results have shown three-fold increase in the phase shifting efficiency)phase-shift per unit length per volt) of simple phase modulators as compared to any previously published material. These results are in reasonable agreement with simple phase modulators as compared to any previously published material.

20. DISTRIBUTION/AVAILABILITY OF ABSTRACT	21. ABSTRACT SECURITY CLASSIFICATION
UNCLASSIFIED/UNLIMITED ☐ SAME AS RPT ☐ DTIC USERS ☐	UUUU

22a. NAME OF RESPONSIBLE INDIVIDUAL	22b. TELEPHONE NUMBER (Include Area Code)	22c. OFFICE SYMBOL
Dr. C. Lee Giles	767-4931	NE

DD FORM 1473, 83 APR   EDITION OF 1 JAN 73 IS OBSOLETE.

USE OF DEPLETION-EDGE TRANSLATION FOR
HIGH-SPEED MODULATION AND SWITCHING OF
LIGHTWAVES: YEAR-1

by

L. A. Coldren, A. Alping, X. S. Wu, T. R. Hausken,
T. C. Huang and J. R. Karin

University of California, Santa Barbara, CA 93106

ANNUAL REPORT: 8/1/85-7/31/86

AFOSR CONTRACT #85-0323

I. Table of Contents

II. Summary

This report describes initial results from the investigation of a new device concept for optical modulators and switches. Applications may be found in optical communication, IC-interconnection and optical computing. The basic concept involves combining and maximizing several effects that can occur in the depletion region of a semiconductor pn-junction to change the index of refraction therein. As a reverse-bias is applied to a properly designed device, the depletion region gets wider and the index shift within it gets larger relative to the surrounding material. The result is that more efficient, compact and potentially higher-speed devices can be realized, since most optical modulation and switching concepts rely upon a change in the index of refraction in some region. Initial results have shown a three-fold increase in the phase shifting efficiency (phase-shift per unit length per volt) of simple phase modulators as compared to any previously published material. These results are in reasonable agreement with simple theoretical predictions. By using the very abrupt impedance discontinuity that occurs at the depletion edge, device configurations that use variable reflection have also been proposed.

In this first year's report, the fabrication and the experimental and theoretical characterization of simple transmission phase modulators are detailed. It is shown that linear electro-optic and free-carrier plasma effects are supplemented by higher-order effects in the high-field region of a doped depletion region. Both carrier and field effects contribute. The experimental structures consist of ridge waveguide samples formed on $Al_{.4}Ga_{.6}As/GaAs$ double-heterostructure material with ~0.2 μm thick GaAs active layers. Phase shifting efficiencies of 61°/V·mm have been measured for the TE mode at 1.06 μm using a GaAs doping of ~2 x 10^{17} cm^{-3}. This figure-of-merit decreases to ~27°/V·mm at 1.53 μm. One-pass losses of less than 2 dB at 1.06 μm have been obtained in samples ~ 0.8 mm long.

III. Objectives

The primary objective of the first year's work was to demonstrate the basic properties of a new kind of phase shifting element which made use of the high fields and depletion of charge in a reverse-biased junction to effect a large effective index change within an optical waveguide. By combining several physical effects, this depletion-edge-translation (DET) element promised to provide larger changes in effective index than possible in previously demonstrated configurations[1,2]. With such elements miniature, highly-efficient optical modulators and switches should be possible.

More specifically for the first year, we set out 1) to fabricate a DET-AlGaAs/GaAs waveguide, 2) to measure the relative index change as a function of voltage and wavelength in it, 3) to model the expected behavior in this configuration and 4) to investigate suitable structures for the implementation of transmission (TDET) and reflection (RDET) modulation and switching devices using this element. In subsequent years, the implementation of practical devices with optimized speed and compatibility for integration has been planned. Recently, the area of application has been more directly focused on components for optical computing.

IV. Progress

In the first year of this work we have substantially met the goals originally set out for the first year's effort. This work has led to several publications and conference reports as listed in the next section. In fact, the performance of our devices is beyond what we had a right to expect, since effects not originally contemplated have helped to increase the measured phase shift. In what follows, we will briefly review the experiments and calculations performed, the results obtained and the potential for future devices that is indicated.

1. Device Configuration and Measurement Apparatus

Figure 1 gives cross sectional and longitudinal schematics of the experimental device configuration used for most of the transmission phase modulator results. Epi-material grown by liquid-phase-epitaxy (LPE) in our lab and metal-organic-chemical-vapor-deposition (MOCVD) at Rockwell in Thousand Oaks, CA were used. A variety of doping levels and active layer configurations are being investigated, but most of the results given here are for active layers of pure GaAs, about 0.25 μm thick, doped n-type to a carrier concentration of 2-3 x 10^{17} cm^{-3}.

The ridge patterns were defined along the [01$\bar{1}$] direction in a layer of thermally grown silicon dioxide or sputtered silicon using a mask containing 5 μm stripes on 300 μm centers. Ridge waveguide structures were then etched by a 1% mixture of bromine in methanol. Some devices were also formed by selective etching of the top AlGaAs cladding layer with HF, leaving a ridge that started at the GaAs active layer. After deposition of an overlayer of silicon dioxide, p-contacts were formed in a window opened at the ridge top. An alloy of Au-Zn was used. After thinning for cleaving, the Au-Ge-Ni n-type contact metallization was deposited on the lower surface. The contacts were then alloyed in forming gas on a graphite strip heater for about two seconds at 430 °C. The samples were then cleaved perpendicular to the ridges to form bars containing several waveguides about 0.5 to 1 mm in length. Bars which visibly looked okay were bonded to a copper mount for testing. Although these reverse biased devices used no static power, soldering to a Cu stud provided heat sinking for accurate temperature control, and it also permitted the use of a

6

forward bias to check for laser operation.
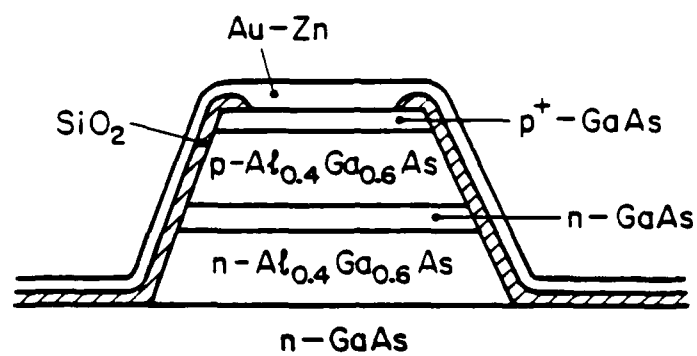

1 (a)
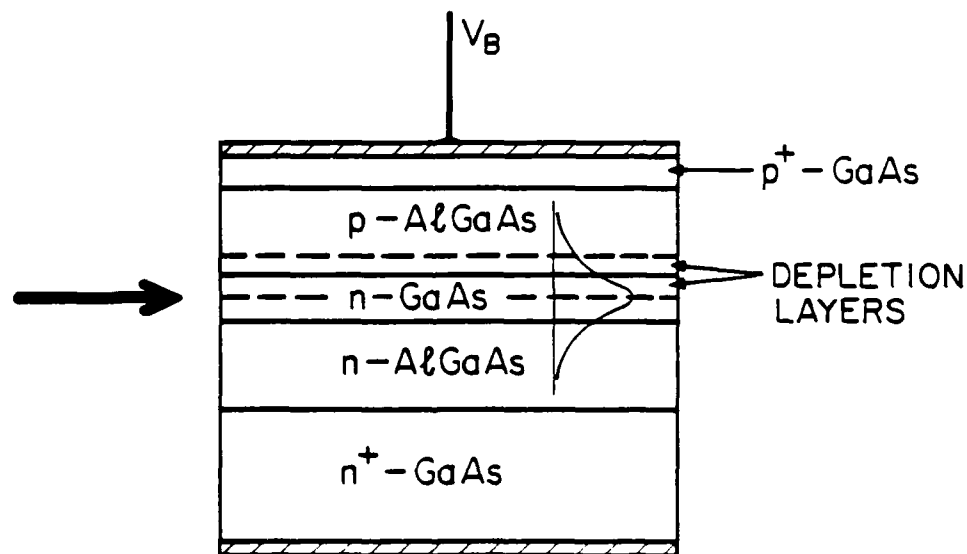
1 (b)

Figure 1. Experimental device configuration. (a) Cross section; (b) longitudinal section.

Figure 2 shows two optical test configurations. Both use the interference of the waveguide signal with a reference beam. The first is a Mach-Zehnder configuration that uses an external reference path. The second makes use of unguided air or substrate modes near the waveguide. Although the first looks better on paper, and some collegues have questioned the reliability of the second, we have not detected any perceptible difference in the measured phase shift in our apparatus using our devices. The second configuration is mechanically much more stable since both reference and signal beams use the same optics. Thus, we routinely use the second scheme for collecting lab data. However, all published results are at least spot checked with the full Mach-Zehnder apparatus.
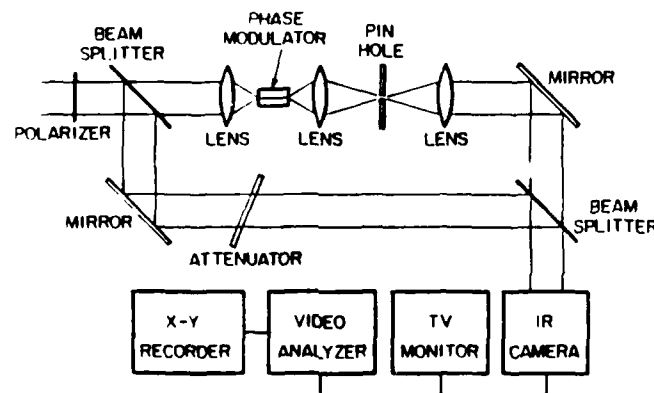
2 (a)
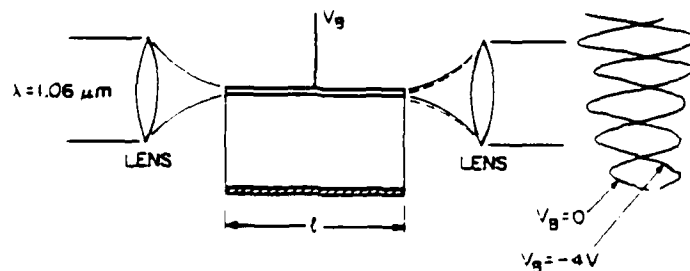
2 (b)

Figure 2. Test configurations. (a) External Mach-Zehnder; (b) internal reference path.

2. Experimental Results

Figure 3 is a plot of the measured phase-shift for both the TE and TM modes at a wavelength of 1.06 μm as a function of applied reverse bias voltage. The device was grown by LPE, and the 0.25 μm active region was doped to about 2×10^{17} cm^{-3}. The device length, l, was 0.74 mm. The data was obtained by recording the magnitude of the fringe patterns at the output of the interferometer shown in Fig. 2 for a number of voltages. This was done with an IR vidicon, a Colorado Video analyser, and an X-Y recorder. The relative displacement of the fringes ΔX gave the relative phase-shift from $\phi = 360° \cdot \Delta X/X_p$, where X_p is the fringe period. From this data we observe a relatively linear phase shift with voltage and normalized phase shifting efficiencies, $\phi/V \cdot l$, of 61° and 40° per Volt-mm respectively for the TE and TM modes. (The reported values[3] of 56° and 38° were in error due to the use of an incorrect length of 0.80 mm.) The voltage for a π-phase shift (V_π) is about 4 V and 6V, respectively.
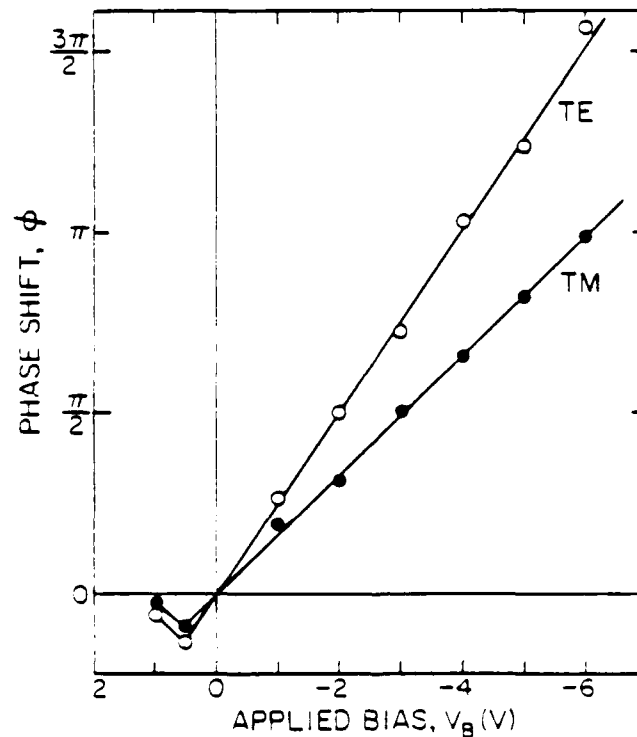
Figure 3. Measured phase shift as a function of applied bias voltage at a wavelength of 1.06 μm. Device length is 0.74 mm; diode reverse breakdown is -6V.

Figure 4 gives measurements similar to Fig. 3 for the TE mode at 1.06, 1.3 and . For the latter two wavelengths, InGaAsP/InP semiconductor lasers were used. The characteristic was approximately linear at 1.3 μm, but it was consistently sublinear at 1.53 μm. As discussed below, it is reasonable to expect some level of nonlinearity since the large shift observed must involve the combination of several different effects, most of which are n

Figure 4. Phase shift versus voltage for three different wavelengths.

Figure 5 summarizes the data versus wavelength for both TE and TM modes. The figure-of-merit (phase-shifting efficiency) drops rapidly for longer wavelengths,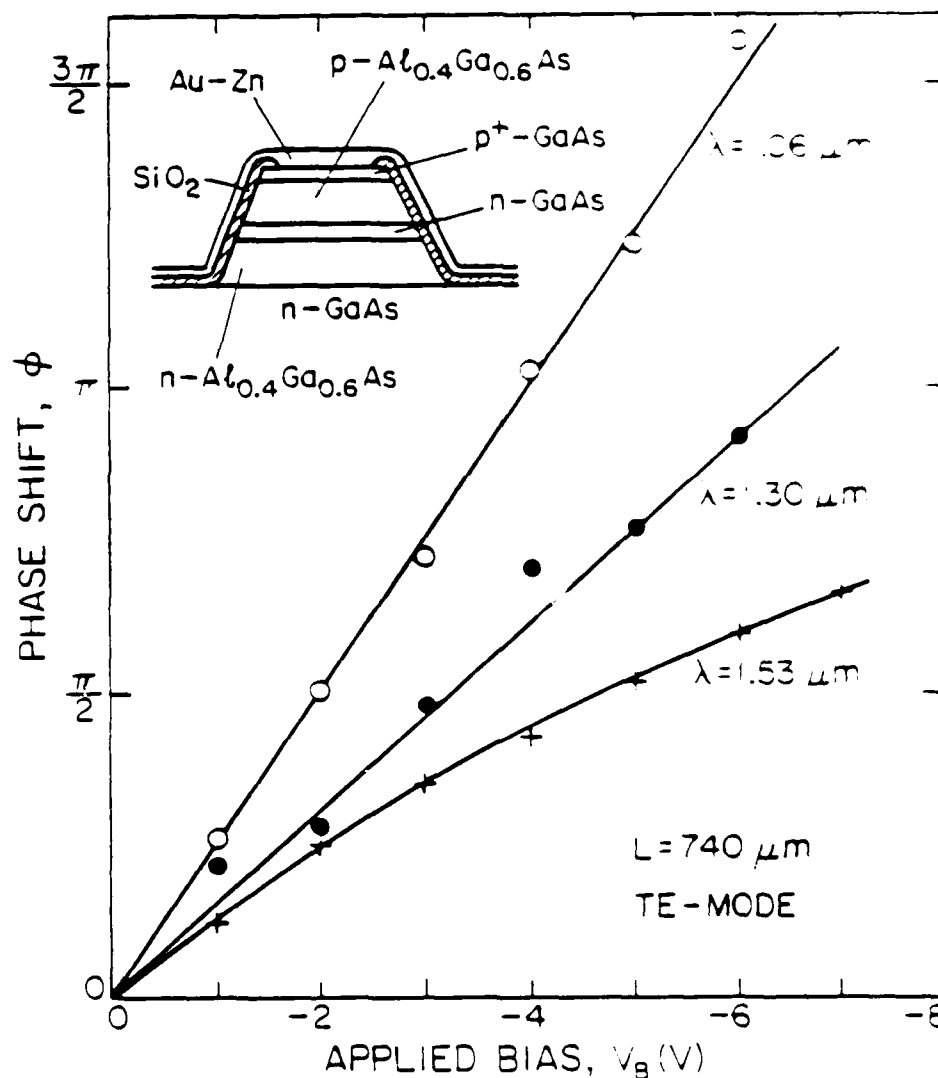 indicating strong effects associated with the absorption edge[4]. The dashed curves are theoretical estimates. Curve (b) is for the free-carrier plasma effect, and curve (a) is for the sum of the linear electro-optic (LEO) effect and the plasma effect. The TM mode should not have any contribution from the LEO effect. The additional phase shift observed is believed to be associated primarily with dispersion effects resulting from several absorption edge shifting phenomena. These will be discussed below. Measurements at 0.89 μm were attempted, but large electro-absorption losses allowed transmission only at forward biases. Additional measurements on devices with different doping levels gave figure-of-merits ranging from 40°/V·mm to 70°/V·mm as the doping was varied from 5 x 10^{16} to 3 x 10^{17} cm^{-3}.
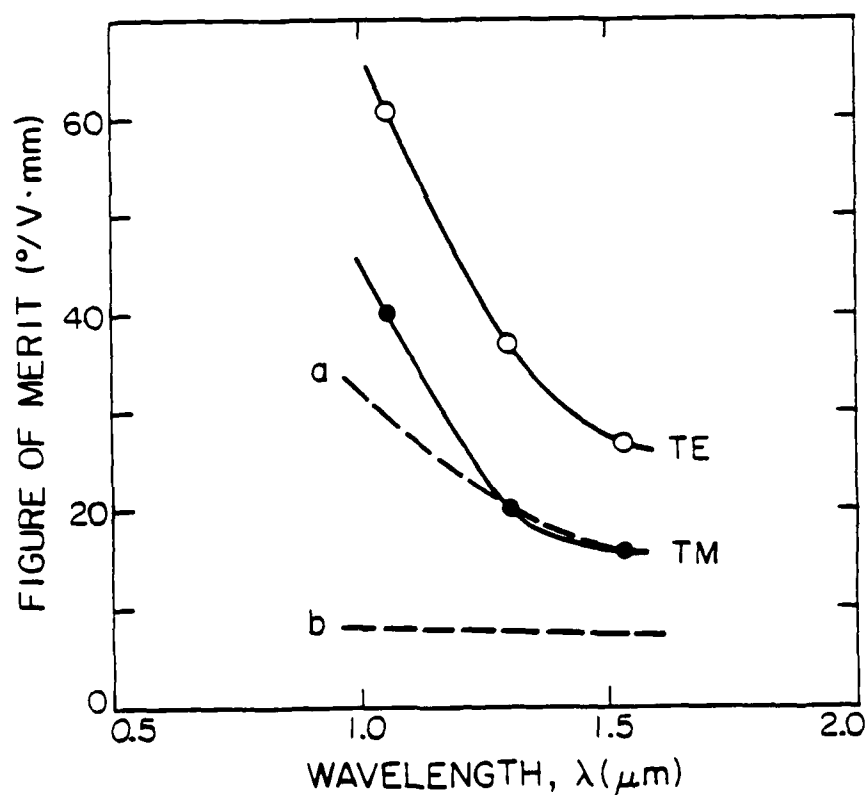
Figure 5. Figure-of-merit for device of Fig. 4. Solid curves: Measured modulator efficiency for both TE andTM modes versus wavelength at 4V. Dashed curves: Calculated contributions from the (a) plasma and LEO effects and (b) the plasma effect alone.

Figure 6 is the direct output amplitude of the TE mode versus voltage without any external interference in another device. In this case, a detector is placed where the upper right-hand mirror is in Fig. 2. The plot is actually the output versus time for an applied linear sawtooth voltage waveform. The amplitude varies periodically with voltage due to the internal interference of the straight-through signal with one that is reflected around the cavity once to acquire three times the phase shift. High-order multiple transits can be neglected if the losses are significant. The result of Fig. 6 allows us to both verify the external interferometer measurements and estimate the internal losses. The ratio of the triple-travel signal to the one-pass signal is $r^2 t^2 \exp(-2j\beta l)$, where r is the facet reflectivity, t is the one-pass amplitude transmission coefficient through the cavity and β is the propagation constant. Thus, from the period and maximum/minimum of the measured output versus voltage, we can obtain the phase shift and internal transmission losses. Actually, it is seen that the voltage for a period, V_p, in this interference is the voltage for a π-phase shift in the one-pass signal, V_π. For the case of Fig. 6 the device has a lower doping (5×10^{16}) and lower figure-of-merit (42°/Vmm for TE at 1.06 μm). Here, we measure $V_p = V_\pi = 10V$. Since the amplitude on this plot is proportional to the optical intensity, we solve for t^2 in terms of the maximum/minimum ratio, I_r, to get $t^2 = (\sqrt{I_r}-1)/[r^2(\sqrt{I_r}+1)]$. From this we calculate a transmission loss of about 1.3 dB in this LPE grown device. Most of this loss is probably due to interface roughness. The free-carrier absorption and electro-absorption at 1.06 μm is estimated to be less than 0.5 dB. Similar measurements on the device of Figs. 3-5 gave a one-pass loss of 8.4 dB, but the measurement may have been flawed by the inclusion of extraneous background light.

The frequency response of these devices is of the utmost importance. Unfortunately, we have been unable to measure the maximum operating frequency allowed by the characteristics of the device itself. To date the experiments have always been limited by the experimental apparatus or mounting fixturing. Thus, we are reluctant to show any results, for fear that they will be interpreted as device limited. However, we can report that the frequency response is flat to beyond 100 MHz. This is noteable because it rules out any thermally related effects that might give a large response near dc but die out at a few KHz.

OPTICAL OUTPUT vs. APPLIED BIAS

(TE-polarization)

Zero level

0   -10   0
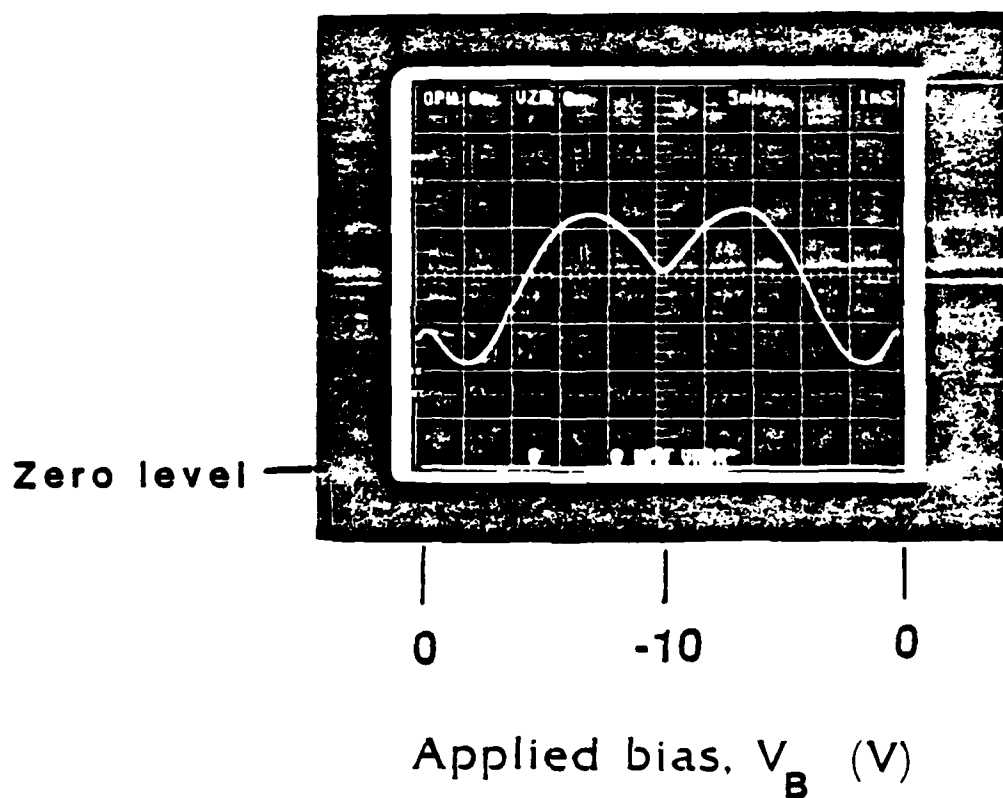
Applied bias, V_B (V)

Figure 6. Intensity-out versus voltage with no facet coatings (no interferometer formed).

3. Discussion of Results

The results given above are believed to be due to the combination of several different effects which, under the proper conditions, can add. We will discuss three different categories: 1) the free-carrier plasma effect, 2) the linear electro-optic effect and 3) the other higher-order, less well-understood effects. As mentioned above, the primary contributor to the latter category is the dispersion associated with absorption edge movement. We will rigorously deal with the first two and make some estimates of contributions to the last catagory, which we will refer to as the quadratic electro-optic effect (QEO) for short. Our measurments, minus effects 1) and 2), are perhaps the best measure of effects in this latter category. These are all modified by the geometry of the guided-wave configuration by a confinement factor, $\Gamma_w(V)$, which gives the fraction of the mode power propagating in the depletion region at applied reverse bias V. Figure 7 is a plot of this confinement factor and the depletion width versus applied bias. The phase shift, $\Delta\phi$, is given by the change in propagation constant, $\Delta\beta$, due to a change in the effective mode index n_{eff} in going from bias V to 0. Or,

$$\Delta\phi = \Delta\beta l = 2\pi\Delta n_{eff} l/\lambda. \tag{1}$$

The net phase shift due to the LEO in the [011] direction is given by evaluating (1)[1],

$$\Delta\phi_{LEO} = [\Gamma_w(V)E_w(V) - \Gamma_w(0)E_w(0)] \cdot \pi n^3 r_{41} l/\lambda , \tag{2}$$

where n = 3.5 is the average refractive index, $r_{41} = 1.4 \times 10^{-12}$ m/V is the appropriate linear electro-optic coefficient in GaAs at 1.06 μm, $E_w(x) = (V_D+x)/w$ is the average field in the doped depletion region of width w at reverse bias voltage x, and V_D is the diffusion potential ~ 1.5 V. Since both $\Gamma_w(V)$ and $E_w(V)$ increase with reverse bias in doped material, we might expect the LEO phase shift to increase more rapidly than linearly with voltage. Plugging numbers into Eq. (2) using Fig. 7 and our device geometry, gives $\Delta\phi \cong 70°$ at 4 V. This is significantly less than half of the measured value at 1.06 μm for the TE mode. Because of symmetry, the LEO effect does not contribute to the TM mode. Thus, the difference between the phase shifts for the TE and TM modes might be due only to the LEO, provided that all other effects affect both modes equally. From Fig. 1 we see that our measured difference at 4 V is about 60°. The descrepency may indicate

that the electro-optic coefficient may be a little smaller than the value used.
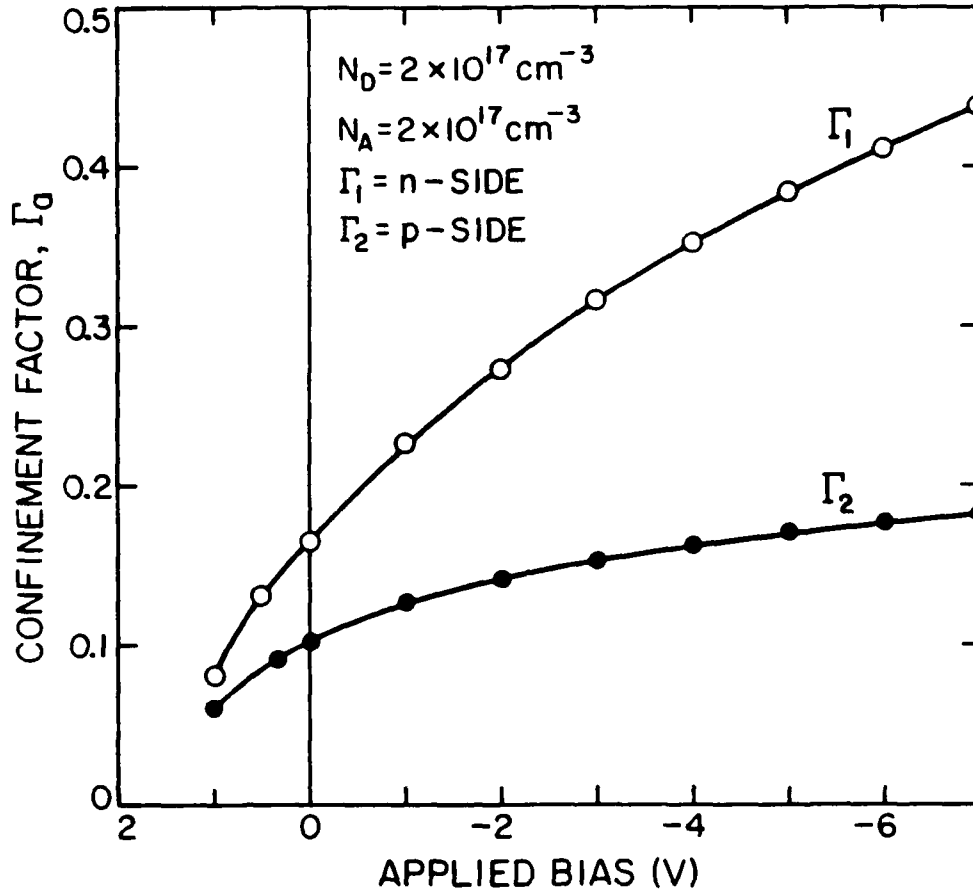

Figure 7. Calculated depletion layer width and depletion layer confinement factor for the configuration of Fig. 1.

The change in propagation phase due to the free-carrier plasma effect occurs as the width of the depletion region increases with reverse bias. That is, we are removing some of the free charge that at zero bias has reduced the effective index for the mode. The index reduction is directly proportional to the concentration of free carriers, N, and wavelength squared, λ^2. The phase change is given by evaluating Δn_{eff} in Eq. (1). In this case the index change Δn in the depletion region is independent of V, and the phase change follows directly after the change in $\Gamma_w(V)$, $\Delta\Gamma$.

$$\Delta\phi_{PL} = 2\pi\Delta\Gamma\Delta nl/\lambda = [\Gamma_w(V) - \Gamma_w(0)] \cdot q^2 nNl\lambda/(4\pi\epsilon c^2 m^*). \qquad (3)$$

where q is the electron charge, ϵ is the dielectric constant, c is the free-space light velocity, m^* is

the effective mass of the carriers and depletion is assumed only in the N-type active region[5]. For GaAs, $\Delta n = \gamma N = (2.14 \times 10^{-21}) \, N$. If we plug-in values at $V = 4 \, V$, $N = N_D = 2 \times 10^{17} \, cm^{-3}$, $1 = 0.74 \, mm$ and $\lambda = 1.06 \, \mu m$, we find $\Delta\phi \cong 15°$. Equation (3) together with Fig. 7 shows that the plasma contribution to the phase shift should increase at a rate less than linearly with voltage, since $\Gamma_w(V)$ increases only as $(V_D + V)^{1/2}$. The sum of the LEO and plasma effects still falls far short of accounting for the measured phase shift. In fact, the unaccounted for portion is the largest component.

In Figure 5 the dashed curve (b) gives the calculated figure of merit due to the plasma effect versus wavelength. This was obtained by dividing Eq. (3) by $V \cdot 1$. Curve (a) is the sum of (b) plus the calculated LEO contribution from Eq. (2) divided by $V \cdot 1$. The other higher-order effects (QEO) must account for the differences between (a) and the TE measurement or (b) and the TM measurement. These two differences are plotted in Fig. 8. They represent the first real measurement of the QEO in this device geometry.

The physical effects that make up this so called QEO are several. The primary constituents are believed to be: 1) band-filling and 2) energy-gap shrinkage due to the large carrier density, and 3) electrorefraction due to the large electric field. That is, there are both carrier and field related effects. Although a detailed investigation still remains to be done, a preliminary calculation based upon a parabolic band approximation[5] gave $\Delta n \sim 0.5 \times 10^{-3}$ with a 6 V bias at 1.06 μm. Or, for our device with $V = 4 \, V$ and $1 = 0.74 \, mm$, $\Delta\phi \cong 90°$, which is in good agreement with the experiment. Thus, we feel that it is reasonable to believe that these effects are major contributors to the phase shift in doped structures near the band-edge. The calculations also suggest that the carrier and field effects each account for about half of the total QEO.

The dependence of the phase shift on field for the QEO can be approximated by a quadratic term in the electric field[3]. This results in an expression of similar form to Eq.(2), except the average field $E_w(V)$ is replaced by the average of the field squared, $E_w^2(V)$, and $n^3 r_{41}/2$ is replaced by ξ, a phenomenological quadratic electro-optic coefficient. Therefore,

$$\Delta\phi_{QEO} = [\Gamma_w(V)E_w^2(V) - \Gamma_w(0)E_w^2(0)] \cdot 2\pi\xi 1/\lambda. \tag{4}$$
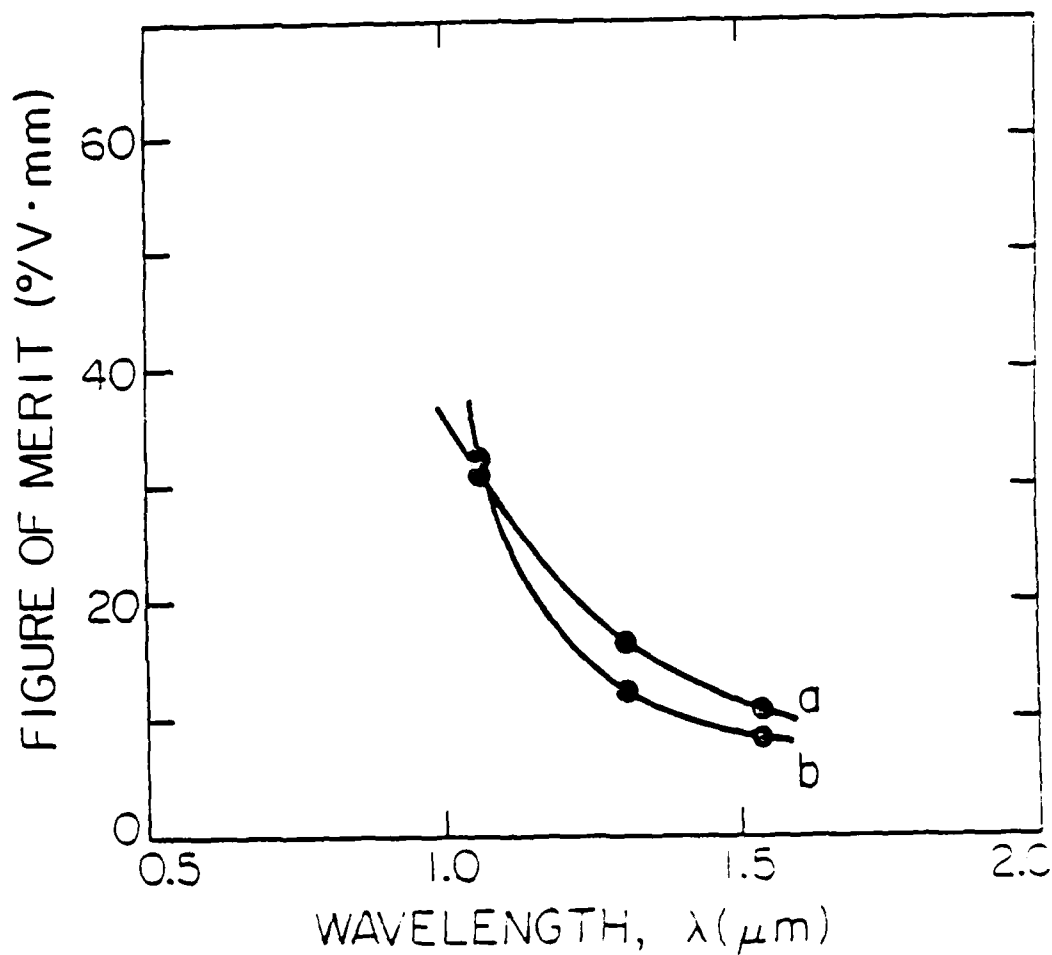
Figure 6. Estimated higher-order contributions to the figure-of-merit from Fig. 5. (a) TE measurement minus the calculated LEO plus plasma effects [dashed curve (a) in Fig. 5]. (b) TM measurement minus the calculated plasma effect [dashed curve (b) in Fig. 5].

4. Design Considerations

In order to optimize the design of a TDET device, we have investigated the effects of the geometry on 1) the figure-of-merit, $\Delta\phi/V\cdot l$, 2) the length for π-phase-shift, L_π and 3) the large signal cut-off frequency, f_c, at this length. The primary independent design parameter is the depletion width w shown in the waveguide schematic of Fig. 9. In this exercise we will assume that the waveguide width d is fixed at a value that provides the minimum mode width, and that w can be varied independent of d and the mode width. The maximum voltage is also assumed fixed, so that we vary w only by changing a pn junction location or the doping level. Later in the examples, we will assume that the applied peak-to-peak rf voltage is limited to 5 V (about 18 dBm), and that a dc bias is applied so that the total applied reverse bias varies from zero to 5 V. That is, we set $V_\pi = 5$ V. As w is reduced, the internal field eventually reaches a breakdown level. Below this point we assume that the voltage is reduced to provide an internal field equal to the breakdown level. Under these assumptions, we can then proceed to calculate the large-signal values of $\Delta\phi/V\cdot l$, L_π, and f_c vs. w for the LEO, the plasma and the QEO effects.
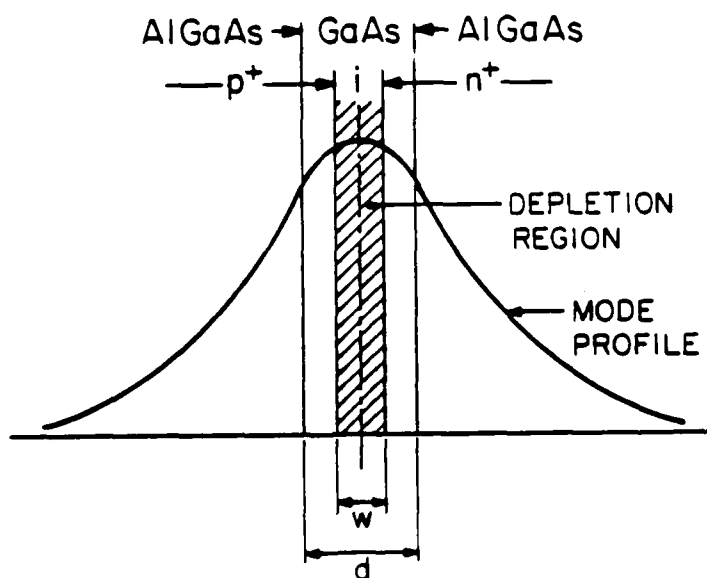

Figure 9. Schematic waveguide cross section showing a mode in a double-heterostructure with guide width d and depletion width w.

For the linear electro-optic effect (LEO) we first assume a pin structure with i-region of width w, so that w and $\Gamma_w(V)$ are independent of voltage. Then from Eq.(2), we find that,

$$\Delta\phi/V\cdot 1 = (\pi n^3 r_{41}/\lambda) \cdot (\Gamma_w/w); \tag{5}$$

$$L_\pi = (\lambda/n^3 r_{41}) \cdot (w/V\cdot\Gamma_w); \tag{6}$$

$$f_c = (n^3 r_{41}/2\pi R\epsilon s\lambda) \cdot (V\cdot\Gamma_w); \tag{7}$$

where $\Gamma_w \equiv \Gamma_w(V)$, R is the source impedence and s is the junction/waveguide lateral width. The first quanities in Eqs. (5-7) are constants for our purposes. The V in the second quantities is also assumed constant for the depletion width greater than the breakdown width, i. e., $w > w_b$. For w $< w_b$, the field is constant at the breakdown level, E_b, so that $L_\pi \propto 1/\Gamma_w$ and $f_c \propto w\cdot\Gamma_w$. If the i-region is doped, Γ_w and w change with voltage, so that,

$$\Gamma_w/w \rightarrow [\Gamma_w(V)/w(V)]\cdot(1+V_D/V) - [\Gamma_w(0)/w(0)]\cdot(V_D/V). \tag{8}$$

For the plasma effect, we assume that the depletion width is adjusted by adjusting the doping. That is, given that the applied reverse bias V is fixed, the doping N_D is set to provide the desired depletion width, w. This leads to a one-to-one correspondence between w and N_D.

$$w = [2\epsilon(V_D+V)/qN_D]^{1/2}, \tag{9}$$

where we have assumed a P^+-N junction. Therefore, from Eq. (3),

$$\Delta\phi/V\cdot 1 = (qn\lambda/2\pi c^2 m^*) \cdot [\Delta\Gamma(V_D/V+1)/w^2]; \tag{10}$$

$$L_\pi = (2\pi^2 c^2 m^*/qn\lambda) \cdot w^2/[\Delta\Gamma(V_D+V)]; \tag{11}$$

$$f_c = (qn\lambda/4\pi^3 c^2 m^* R\epsilon s) \cdot [\Delta\Gamma(V_D+V)/w]. \tag{12}$$

Again, the last quantity includes all the terms that vary with w. Also as above, the voltage is assumed fixed for depletion widths greater than the breakdown width, w_b. Below this ($w < w_b$), the field is kept fixed at the breakdown level. Thus, $(V_D+V)/w \rightarrow E_b$.

For the quadratic electro-optic effect (QEO), we again first assume a pin structure, so that Γ_w and w are independent of applied bias. Then Eq.(4) and this assumption give,

$$\Delta\phi/V\cdot 1 = (2\pi\xi/\lambda) \cdot [\Gamma_w(V+2V_D)/w^2]; \tag{13}$$

$$L_\pi = (\lambda/2\xi) \cdot w^2/[\Gamma_w V(V+2V_D)]; \tag{14}$$

$$f_c = (\xi/\pi R\epsilon s\lambda) \cdot [\Gamma_w V(V+2V_D)/w]. \tag{15}$$

If the active region is doped, then,

$$\Gamma_w V(V+2V_D)/w^2 \rightarrow \Gamma_w(V)(V+V_D)^2/w^2(V) - \Gamma_w(0)V_D^2/w^2(0). \qquad (16)$$

Again, for $w < w_b$, the voltage is reduced to maintain the field at its breakdown level, or $(V+V_D)/w$ $\rightarrow E_b$.

In order to appreciate the importance of Eqs.(5-16), we have plotted the depletion-width confinement factor, Γ_w, the figure-of-merit, $\Delta\phi/V\cdot l$, the length required for π-phase shift, L_π, and the large-signal cut-off frequency, f_c, versus w for specific examples in Figs. 10-13, respectively. For these calculations we assume a voltage swing of $V_\pi = 5V$, an $Al_xGa_{1-x}As/GaAs$ double-heterostructure with x=0.4, a GaAs layer thickness, d=0.2 μm, a guide width of 3 μm, a wavelength of 1.06 μm, and a breakdown field of 4×10^5 V/cm. The LEO and plasma characteristics are calculated from well-known constants; the QEO proportionality constant, ξ, is adjusted for approximate agreement with our experimental results reported above. The axis opposite w gives the doping required to obtain w at 5 V for the plasma effect. In Figs. 11-13 the individual contributions are plotted along with a net characteristic (labeled Σ) that would result if all effects were present in one device. However, since the LEO & QEO characteristics are calculated for a pin structure, and the plasma curves are for a doped active region, the Σ curve gives only a general trend. Future calculations will give the exact net effect.

From Fig. 11 we see that the LEO dominates at large w (small fields) and that the QEO is largest at small w (large fields). The figure-of-merit for all effects increases as $w \rightarrow 0$, since the internal field is increasing for $w > w_b$, and V decreases for $w < w_b$. For large w (where $\Gamma_w \rightarrow 1$), the LEO figure-of merit decreases as 1/w, and the plasma and QEO characteristics decrease as $1/w^2$. The kink apparent in the QEO and Σ curves is due to the switch-over from constant voltage to constant field at $w = w_b$. This same kink is more noteworthy in Figs. 12 and 13.

Figure 12 shows that the minimum device length will occur at $w = w_b$. The minimum $L_\pi \cong$ 0.4 mm in the current example. Also, this minimum is relatively sharp, so that the use of a larger w is costly in terms of device length. For large w, the required length must increase linearly with w for the LEO and quadratically with w for the plasma and QEO. Figure 13 shows that the

maximum cut-off frequency also occurs at relatively small w. In our example, $w(f_c = f_{cmax}) \cong 0.4$ μm. This might come as a surprise, if one is unaccustomed to dealing with the realistic case of limited modulation voltage and the presence of higher-order effects. Conventional wisdom suggests that the capacitance per unit length should be kept small by using a relatively large w. But, we see that the existence of the plasma and QEO phenomena suggest a lower value than one would choose with the LEO alone.
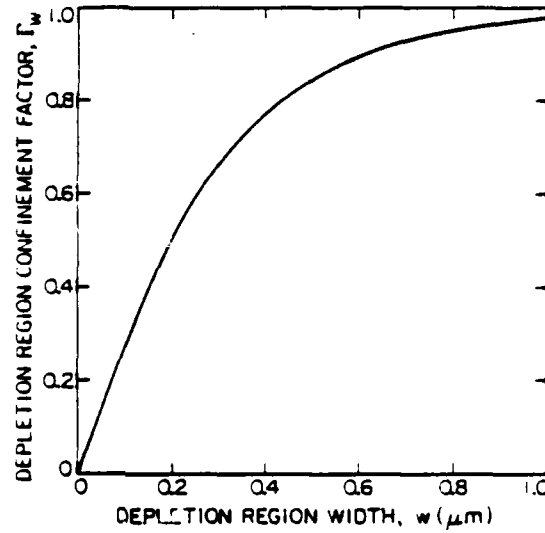

Figure 10. Depletion-width confinement factor versus depletion width.
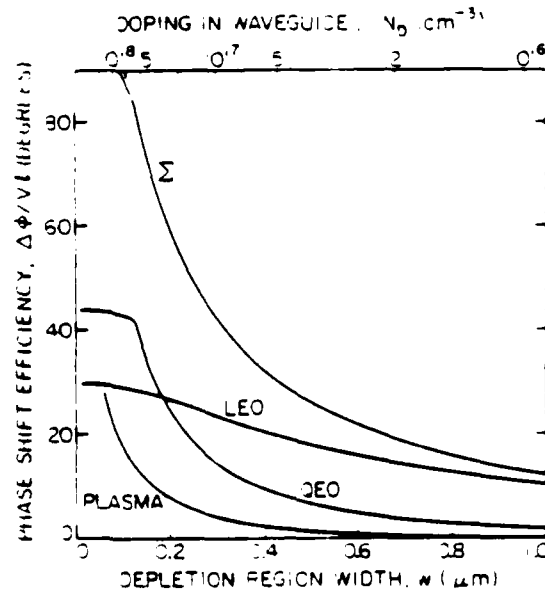

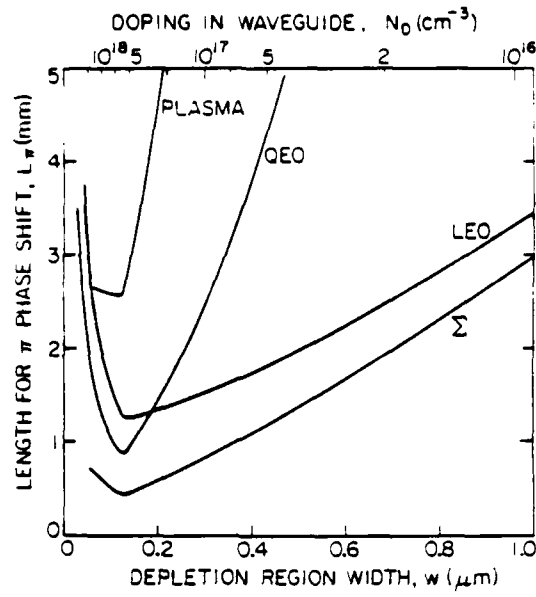Figure 11. Theoretical figure-of-merit versus depletion width.

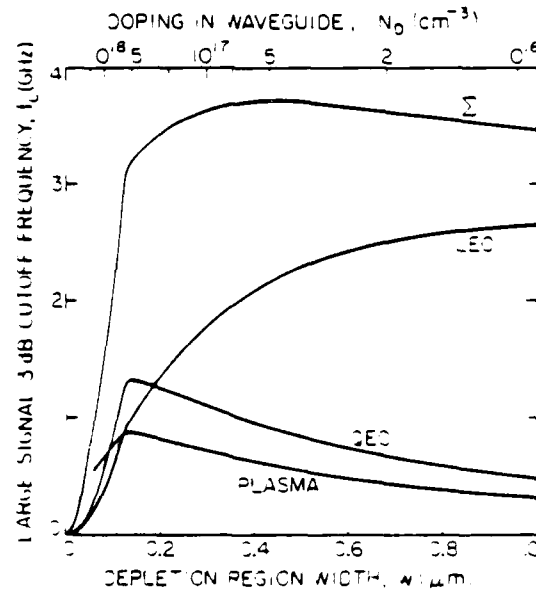Figure 12. Theoretical length for π-phase shift versus depletion width.

Figure 13. Theoretical large-signal cut-off frequency versus depletion width.

5. Future Prospects

In the above we have shown that it is possible to obtain higher efficiency and speed than possible with the linear electro-optic effect alone. In fact, at present these results represent record levels for a reverse biased configuration. However, we feel that there is still much room for further progress in this area. The next basic area to be introduced is that of multi-quantum-well (MQW) structures. At this writing, we already have begun work with these structures using material supplied by Rockwell International, Thousand Oaks, CA. It is already clear that the field dependent higher-order effects are strong in MQW structures. It remains to be seen just how strong they are compared to those already studied.

In addition to maximizing the underlying physical effects, the time is ripe to make more complete device structures. The masks have already been made for Mach-Zehnder interferometer modulators and total-internal-reflection switches. These devices will be made and studied during 1987. Also, it has been decided to focus on devices for optical computing. Multilayer devices that are particularly well suited for a propagation path normal to the surface have been proposed. Using the highly-efficient phase shifting elements demonstrated above, or the MQW structures under study, new levels of performance should be possible.

6. References

1. F.K. Reinhart and B.I. Miller, "Efficient GaAs-AlGaAs double-heterostructure light modulators," Appl. Phys. Lett., 20, 36-38 (1972).

2. A.J.N. Houghton, P.M. Rodgers and D.A. Andrews, "High-performance GaAs-GaAlAs phase modulators for PSK optical fibre systems," Elect. Lett., 20, 479-480 (1984).

3. A. Alping, X.S. Wu, T.R. Hausken and L.A. Coldren, "Highly efficient waveguide phase modulator for integrated optoelectronics," Appl. Phys. Lett., 48, 1243-1245 (1986).

4. A. Alping and L.A. Coldren, "Electro-refraction in GaAs and InGaAsP and its application to phase modulators," submitted to J. of Appl. Physics.

5. J.G. Mendoza-Alvarez, F.D. Nunes and N.B. Patel, "Refractive index dependence on free carriers for GaAs," J. Appl. Phys., 51, 4365-4367 (1980).

V. Publications: 8/85 - 9/86

1. X.S. Wu, A. Alping, A. Vawter and L.A. Coldren, "Miniature optical waveguide modulator in AlGaAs/GaAs using carrier depletion," Electron. Letts., 22, 328-329 (February 1986).

2. A. Alping, X.S. Wu, T.R. Hausken and L.A. Coldren, "Highly efficient waveguide phase modulator for integrated opto-electronics," Appl. Phys. Letts., 48, 1243-1245, (May 1986).

3. A. Alping and L.A. Coldren, "Electro-refraction in GaAs and InGaAsP and its application to phase modulators," submitted to Jrnl. Appl. Physics.

VI. Talks & Other Interactions

Conference Talks:

1. X.S. Wu, A. Alping, T.R. Hausken and L.A. Coldren, "Highly efficient waveguide phase shifter for integrated optoelectronics," 1986 CLEO Digest, San Francisco, Paper MF3 (June 1986).

2. L.A. Coldren, A. Alping, X.S. Wu and G.A. Vawter, "Use of depletion for optical channel waveguide phase modulators with record efficiency," 1986 Device Research Conference Proceedings, Paper VA-4, Amherst MA (June 1986).

3. A. Alping, X.S. Wu and L.A. Coldren, "Wavelength dependence of high performance AlGAAs/GaAs depletion-edge-translation waveguide phase modulators," submitted to the Integrated Optics and Optical Communication Conference.

Seminars:

1. L.A. Coldren, "Processing techniques for integrated Optoelectronics," GaAs Seminar IBM Research Labs, Yorktown Heights (October 1985).

2. L.A. Coldren, "Fabrication of high-speed optoelectronic devices," Departmental Seminar, Los Alamos National Labs, Los Alamos (November 1985).

3. L.A. Coldren, "Technology for high-speed optoelectronic devices," Departmental Seminar, Sandia National Labs, Sandia, (February 1986).

Professor Coldren is a consultant at Rockwell International in Thousand Oaks for Derek Cheung, Director of the Electro-optics Lab. Rockwell has supported the program by supplying MOCVD wafers.

VII. Personnel

1. Professor Larry A. Coldren, PhD: Principal investigator. 15% time.
    Dr. Coldren got his doctorate from Stanford University in 1972. He spent the next twelve
    years at Bell Labs before moving to the University of California at Santa Barbara in 1984. He
    holds 21 patents in the areas of surface-acoustic-wave signal processing devices,
    microfabrication processes and III-V compound optoelectronic devices for optical
    communication and processing. He has over 100 journal publications in these same areas.
    His current interests are in the areas of optical communication, optical computing and
    microfabrication technology. In this project Dr. Coldren contributed the basic ideas and
    research management.

2. Dr. Arne Alping, PhD: Visiting research engineer. 80% time.
    Dr. Alping got his doctorate from Chalmers University in Sweden in 1984. After completing
    a post doctoral appointment there, he joined UCSB 10/1/85 for a one year appointment as a
    visiting researcher. His current interests are in digital and coherent optical communications.
    In this project Dr. Alping was responsible for leading and training students, making the
    optical measurements and performing the theoretical calculations.

3. D. X. S. Wu, PhD: Visiting research engineer. 50% time.
    Dr. Wu received his doctorate from the Shanghai Institute of Metallurgy in 1963. Since that
    time he has worked on various projects involving the liquid-phase-epitaxial growth of
    AlGaAs/GaAs and InGaAs/InP for optoelectronic devices. He joined UCSB on 7/1/85 for
    18 months as a visiting scholar. In this project Dr. Wu was responsible for leading and
    training students and fabricating some of the experimental devices.

4. Mr. T. R. Hausken: Research Assistant. 100% summer; 50% academic time.
    Mr. Hausken received his B.S.E.E. from Montana State University in 1979. He spent
    the next five years at Texas Instruments first with ac plasma display development, and
    later with MOS memory failure analysis. He began studies at UCSB in 1/85 and was
    responsible for fabrication and testing of optical devices.

5. Mr. T. C. Huang: Research Assistant. 100% summer; 50% academic time.
    Mr. Huang received his B.S. Physics from Jilin University in the People's Republic of
    China in 1982. He began studies at UCSB in 9/84 and received his M.S.E.E. in 1986.
    Mr. Huang was responsible for device fabrication and measurements.

6. Ms. J. R. Karin: Research Assistant. 50% summer time.
    Ms. Karin received her B.A. in Physics from Mount Holyoke College in 1983. She spent two
    years at AT&T Bell Laboratories in the Quantum Physics and Electronics Research
    department doing research in picosecond optoelectronics. She has been at UCSB since
    9/85, and was responsible for some of the device characterization.

VIII. New Discoveries

The concept of the depletion-edge translation modulator and switch was patented by the
University of California before the program was funded.

END
3-87
DTIC